AIP | The Journal of Chemical Physics

The importance of accurate adiabatic interaction potentials for the correct description of electronically nonadiabatic vibrational energy transfer: A combined experimental and theoretical study of NO(v = 3) collisions with a Au(111) surface

Kai Golibrzuch, Pranav R. Shirhatti, Igor Rahinov, Alexander Kandratsenka, Daniel J. Auerbach, Alec M. Wodtke, and Christof Bartels

Citation: The Journal of Chemical Physics **140**, 044701 (2014); doi: 10.1063/1.4861660
View online: http://dx.doi.org/10.1063/1.4861660
View Table of Contents: http://scitation.aip.org/content/aip/journal/jcp/140/4?ver=pdfcov
Published by the AIP Publishing

The importance of accurate adiabatic interaction potentials for the correct description of electronically nonadiabatic vibrational energy transfer: A combined experimental and theoretical study of NO($v = 3$) collisions with a Au(111) surface

Kai Golibrzuch,[1,2] Pranav R. Shirhatti,[1,2] Igor Rahinov,[3] Alexander Kandratsenka,[1,2] Daniel J. Auerbach,[1,2,4] Alec M. Wodtke,[1,2] and Christof Bartels[1,2]
[1]*Institute for Physical Chemistry, Georg August University of Göttingen, Göttingen 37077, Germany*
[2]*Max Planck Institute for Biophysical Chemistry, Göttingen 37077, Germany*
[3]*Department of Natural Sciences, The Open University of Israel, Ra'anana 4353701, Israel*
[4]*Department of Chemistry and Biochemistry, University of California Santa Barbara, Santa Barbara, California 93106, USA*

(Received 26 September 2013; accepted 20 December 2013; published online 22 January 2014)

We present a combined experimental and theoretical study of NO($v = 3 \rightarrow 3, 2, 1$) scattering from a Au(111) surface at incidence translational energies ranging from 0.1 to 1.2 eV. Experimentally, molecular beam–surface scattering is combined with vibrational overtone pumping and quantum-state selective detection of the recoiling molecules. Theoretically, we employ a recently developed first-principles approach, which employs an Independent Electron Surface Hopping (IESH) algorithm to model the nonadiabatic dynamics on a Newns-Anderson Hamiltonian derived from density functional theory. This approach has been successful when compared to previously reported NO/Au scattering data. The experiments presented here show that vibrational relaxation probabilities increase with incidence energy of translation. The theoretical simulations incorrectly predict high relaxation probabilities at low incidence translational energy. We show that this behavior originates from trajectories exhibiting multiple bounces at the surface, associated with deeper penetration and favored (N-down) molecular orientation, resulting in a higher average number of electronic hops and thus stronger vibrational relaxation. The experimentally observed narrow angular distributions suggest that mainly single-bounce collisions are important. Restricting the simulations by selecting only single-bounce trajectories improves agreement with experiment. The multiple bounce artifacts discovered in this work are also present in simulations employing electronic friction and even for electronically adiabatic simulations, meaning they are not a direct result of the IESH algorithm. This work demonstrates how even subtle errors in the adiabatic interaction potential, especially those that influence the interaction time of the molecule with the surface, can lead to an incorrect description of electronically nonadiabatic vibrational energy transfer in molecule-surface collisions. © *2014 AIP Publishing LLC*. [http://dx.doi.org/10.1063/1.4861660]

I. INTRODUCTION

A quantitative understanding of interactions between molecules and surfaces in microscopic detail is important for a variety of chemical processes at surfaces, many of which are central to heterogeneous catalysis. The energy exchange between surface degrees of freedom and molecular vibration is of particular interest, as the vibrational motion is most closely related to molecular dissociation, that is, to chemical reaction. For certain systems, the Born-Oppenheimer approximation[1] fails, and the molecular vibration can directly couple to electronic degrees of freedom. Such nonadiabatic coupling between molecular vibration and electron-hole pair excitation of the solid can have significant or even dominant influence on vibrational energy transfer.[2–4]

Early experimental evidence for Born-Oppenheimer breakdown is available for adsorbates at metal surfaces. CO molecules adsorbed on metal surfaces such as Cu, Pt, or Ru have vibrational lifetimes on the order of picoseconds,[5–7] compared to millisecond lifetimes observed for CO adsorbed on NaCl.[8] The theoretical picture that was developed explains the strong vibrational damping by a transient population of the molecular affinity level, which is lowered in energy and broadened as the molecule comes close to the metal surface.[9] The vibrational lifetimes could also be reproduced by electronic friction (EF) theory, which describes the dissipation of vibrational energy by frictional forces that involve energy exchange with the electronic degrees of freedom of the metal.[10]

Using molecular beam–surface scattering, the dynamics of molecule-surface interactions can be probed with quantum state resolution, and various systems have been investigated with this approach. There is strong evidence for electronically nonadiabatic interaction in the collision-induced vibrational excitation of NO/Ag(111), NO/Cu(110), CO/Au(111), and HCl/Au(111).[11–14] A one-dimensional Newns-Anderson model explains the incidence-energy and surface-temperature

dependence of the vibrational excitation probability for NO/Ag(111).[15] In this model, the vibrational excitation of the molecule is due to de-excitation of thermal electron-hole pairs in the metal.

NO scattering from Au(111) is one of the most extensively studied model systems for electronic nonadiabaticity, both experimentally and theoretically. Experimental results showed that NO in high vibrational states ($v_i = 15$), incident with translational energy of 0.05 eV, relax into a broad range of vibrational states when scattered from a gold surface.[16] Several different theoretical approaches semi-quantitatively reproduce the observed vibrational state distributions, including a Monte Carlo model with stochastic quantum jumps between the neutral and negative ion states of the molecule,[17] fully quantum mechanical first-principles EF theory,[18] and molecular dynamics (MD) employing Independent Electron Surface Hopping (IESH) on a density functional theory (DFT) based Newns-Anderson Hamiltonian.[19–22]

In order to attempt to distinguish between these various theoretical approaches, a comprehensive series of experiments was performed to study the collision-induced vibrational excitation of NO($v = 0$) into vibrational states $v = 1,\ 2$ when scattered from a Au(111) surface over a wide range of incidence energies and surface temperatures (300 K $\leq T_s \leq$ 1000 K and 0.11 eV $\leq E_i \leq$ 1.05 eV).[23] The surface-temperature dependence of the absolute vibrational excitation probabilities follows Arrhenius functions with apparent activation energies equal to the vibrational excitation energies, suggesting that the energy for vibrational excitation is taken from a thermal bath – namely, the surface electronic system – rather than from the translational energy of incidence.[24,25] The excitation probabilities for $v = 0 \rightarrow 1,\ 2$ increase with incidence translational energy[23] due to a deeper penetration of fast molecules into regions of stronger nonadiabatic interaction.[11,15] A detailed comparison of experimental results to IESH-based simulations showed good semi-quantitative agreement over the entire range of experimental conditions, whereas electronic friction based simulations failed completely.[26] Despite this unprecedented success, the IESH-based simulations deviated from experiment in a systematic way: they predicted a dependence of vibrational excitation on incidence energy of translation that was somewhat weaker than that seen experimentally. Subsequent work at a single incidence energy also showed the IESH-based simulations underestimated the amount of NO($v = 0 \rightarrow 3$) excitation.[25]

In light of these albeit rather small discrepancies between the predictions of the IESH-based simulations and experimental observations, we set about to design new experiments that might more rigorously test the strengths and weaknesses of the IESH-based approach. For reasons that are far from obvious and will be now explained, we settled on NO($v = 3$) vibrational relaxation as the ideal test case. There are several reasons for this.

First, only one experiment on the vibrational relaxation of NO in lower vibrational states has been previously reported. In that experiment, NO($v = 2$) was scattered from a Au(111) surface, and both excitation to $v = 3$ and relaxation to $v = 1$ were observed.[27] For both channels, the transition probabilities increase with incidence energy of translation over the range of 0.10–0.72 eV. To our knowledge, no comparison of these data to theoretical models is available.

Second, vibrational relaxation provides several advantages over vibrational excitation in comparing experiment to first-principles theories of nonadiabatic interaction of molecules with metal surfaces. Vibrational relaxation rates are essentially independent of surface temperature. The temperature dependence, which mainly reflects the statistical mechanics of electron-hole pair excitation, is not a dynamically interesting quantity. By contrast, the dependence on incidence energy of translation directly probes how the strength of nonadiabatic interaction depends on the nature of the molecule-surface collision. Hence, comparisons of experiment and theory for vibrational relaxation represent a fundamentally simpler way to explore nonadiabatic dynamics. Another advantage is that relaxation probabilities can be large (i.e., greater than 0.1). By contrast excitation probabilities are typically small as they are limited by the thermal population of electron-hole pairs. For example, electronically nonadiabatic vibrational excitation probabilities for HCl($v = 0$) can be less than 10^{-5}.[13] Typically, simulations of rare events are computationally intensive, and molecular dynamics with IESH or EF are not exceptional. Far fewer trajectories are needed to make statistically meaningful comparison to experiment for relaxation than for excitation.

The absence of NO dissociation is a third reason why NO($v = 3$) relaxation is ideal. One might naively expect that electronically adiabatic interactions do not play an important role in the theoretical treatment of electronically nonadiabatic energy transfer in molecular collisions at metal surfaces. This view ignores the fact that modern approaches to electronically nonadiabatic energy transfer rely on adiabatic input to describe the dynamics. For example, if, as is likely, the DFT-derived adiabatic interaction potential for NO/Au(111) used in the IESH simulations of Ref. 21 for NO($v = 15$) relaxation does not accurately describe NO dissociation, comparison to experiment can be misleading. This is a particular concern in light of recent calculations that place the activation energy for NO dissociation on Au(111) near 3.5 eV,[28] which is close to the vibrational energy of NO($v = 15$). As DFT is known to sometimes have problems in the accurate determination of activation energies, one should consider a test of electronically nonadiabatic theories that is expected to be less sensitive to such errors in the adiabatic interaction potential. Hence we have been motivated to investigate the NO/Au collision system at low levels of vibrational excitation, $v = 1,\ 2,\ 3$.

There is a fourth reason to look at low v states: Molecular dynamics with both IESH and EF were able to explain experimental results on the vibrational relaxation of NO($v_i = 15$), at least at one incidence translational energy.[18,22] Distinguishing the two theories is fundamental to understanding the nature of electronically nonadiabatic interactions. Here, it is important to understand that friction theory, which is based on harmonic-oscillator and weak-coupling approximations, assumes that vibrational relaxation of NO(v_i) proceeds sequentially via the vibrational states $v_i - 1$, $v_i - 2$, and so on, and that the coupling strength between neighboring vibrational levels v and $v + 1$ scales linearly with v_i.[18] This

latter feature of the theory is probably essential to reproducing the large experimental vibrational relaxation probabilities for NO($v_i = 15$). It is not clear if EF-based models can also explain relaxation from lower vibrational states, where the coupling strength is much weaker. Finally, it was argued that the IESH theory unifies our picture of energy transfer for NO/Au(111) scattering for vibrational excitation of $v = 0$ and vibrational relaxation of $v = 15$.[26] The application of the same model to NO($v = 3 \rightarrow 3,\ 2,\ 1$) relaxation is an obvious additional test.

In this paper, we present measurements of the branching ratios for the scattering of NO($v = 3$) from a Au(111) surface at incidence energies from 0.12 to 1.07 eV, into final vibrational states $v = 3,\ 2,\ 1$. The experimental data are compared to state-to-state scattering probabilities derived from electronically adiabatic MD simulations as well as two approaches to electronically nonadiabatic molecular dynamics (IESH[22,26] and EF[26]). We find significant disagreement between observation and all three theoretical models. While the failure of adiabatic MD and EF comes as no surprise, the highly successful IESH-based approach, which relies on a DFT-derived Newns-Anderson Hamiltonian, also fails to accurately describe the translational energy dependence of the vibrational energy transfer probabilities. Furthermore, the disagreement is much more serious than that reported in Ref. 26.

In order to better understand the origin of these deficiencies, we performed a detailed analysis of simulated trajectories over this range of incidence energies. We identify one important source of disagreement between experiment and theory: The molecular dynamics simulation does not correctly describe the single-bounce (direct scattering) nature of the interaction. That is, multi-bounce trajectories, which are inconsistent with experimental observation, influence the energy transfer dynamics. Furthermore, the multi-bounce artifacts are more important at low incidence energy of translation. By artificially selecting only single-bounce trajectories, the agreement with experiment is improved. These multi-bounce artifacts are present in our IESH-based simulations as well as in EF and even adiabatic simulations. This result points out a very subtle point: a correct description of the weak forces associated with the adiabatic interaction potential, even when the total energy is far below the dissociation threshold, can be critically important to predict electronically nonadiabatic vibrational energy transfer. Errors in the adiabatic interaction potential that lead to unrealistically long interaction times enhance electronically nonadiabatic vibrational energy exchange. This underlines the importance of accurate adiabatic calculations that correctly describe translational inelasticity, translation-to-phonon coupling, potential energy surface corrugation, and dynamical steering.

II. METHODS

A. Experimental setup

The experimental apparatus has been described in detail previously.[29] Briefly, a pulsed molecular beam, with pulse duration of approximately 70 μs, is generated in a supersonic expansion using a piezo-electric pulsed valve at 3 bars stagnation pressure. The beam is skimmed and passes two stages of differential pumping before it enters the ultra-high vacuum (UHV) chamber, whose base pressure is 1.5×10^{-10} Torr, rising to 2×10^{-9} Torr when the molecular beam is on. From the geometry of the experiment, we calculate the beam divergence to be 1.2°. Inside the UHV chamber the beam is scattered off the (111) surface of a gold single crystal at near normal incidence (incidence angle $\theta_i \approx 2°$ with respect to the normal). The UHV chamber is equipped with a simple time-of-flight (TOF) mass spectrometer consisting of a repeller plate, an ion lens with two cylindrical elements and a dual microchannel plate detector. Prior to each measurement the Au(111) crystal is cleaned by argon ion bombardment, inspected for impurities using Auger electron spectroscopy (AES), and finally annealed at 1000 K to recover the (111) surface structure.

We use the frequency doubled output of a Nd:YAG pumped pulsed dye laser (0.1 cm^{-1} bandwidth, 233–250 nm, 2–3 mJ) for (1+1) resonance enhanced multiphoton ionization (REMPI) of NO via the A $^2\Sigma^+$ state. In addition, we employ a high intensity narrow bandwidth (0.005 cm^{-1}) IR system which has been described in detail recently.[30] Briefly, a cw Nd:YLF laser pumps a single-mode cw ring dye laser, which seeds a five-stage pulse amplifier pumped by the second harmonic of an injection seeded Nd:YAG laser. The pulse amplification produces intense Fourier-transform limited nanosecond pulses (35 mJ, 669 nm) which are used for difference frequency mixing with 130 mJ of the Nd:YAG fundamental to generate 1.8 μm IR radiation (3–5 mJ). These pulses are further amplified by optical parametric amplification (OPA) with additional 280 mJ of the seeded Nd:YAG fundamental, resulting in intense IR pulses (up to 30 mJ) with nearly transform limited bandwidth (<130 MHz) at 1.8 μm.

To produce vibrationally excited molecules in the incident molecular beam, we use the 0–3 R(0.5) second overtone transition at 5548.875 cm^{-1}. We stabilize the pump laser frequency to within 0.005 cm^{-1} by measuring the wavelength of the dye laser and the Nd:YAG laser with a wavemeter (HighFinesse WS/7 with multi-channel switch) and using the calculated IR frequency as a feedback for the ring dye laser. The IR laser beam runs parallel to the face of the Au crystal crossing the molecular beam at a distance of 14 mm from the Au surface. We use a 50 cm focal length cylindrical lens to focus the IR beam to excite a thin cylindrical slice of the molecular beam. The diameter of the cylindrical excitation volume is 1 mm (determined by the collimation of the molecular beam) and its thickness is 0.1 mm (determined by the focus of the IR laser). The unfocused UV ionization laser beam runs parallel to the IR beam but is 10 mm from the surface. This beam is displaced about 3.5 mm perpendicular to the molecular beam, corresponding to a scattering angle of 19°, to avoid ionization of NO in the incident beam. We use the 0–1, 0–2, and 1–3 bands of the A $^2\Sigma^+ \leftarrow$ X $^2\Pi$ transition to detect molecules in vibrational states $v = 1$, 2, and 3. For the 0–1 band, we observe significant background resulting from vibrationally elastic scattering of thermally populated NO($v = 1$) in the incident beam as well as from

TABLE I. Parameters for the gas mixtures used in this study. All velocity distributions were fit to flowing Maxwell distributions, $f(v) \propto v^3 \exp[-(v - v_0)^2/\sigma^2]$.[36] The fit parameters v_0 and σ, the mean velocity $\langle v \rangle$, and energy $\langle E \rangle$ as well as the respective full width at half maximum (FWHM) values are given.

Mixing Ratio	v_0 (m/s)	σ (m/s)	$\langle v \rangle$ (m/s)	FWHM (m/s)	$\langle E \rangle$ (eV)	FWHM (eV)
10% NO/90% N_2	858	61	865	102	0.12	0.03
6% NO/24% N_2/70% H_2	1296	84	1304	139	0.27	0.06
15% NO/85% H_2	1563	98	1572	163	0.39	0.08
9% NO/91% H_2	1824	81	1829	135	0.52	0.08
6.5% NO/93.5% H_2	2037	130	2049	216	0.65	0.14
3% NO/97% H_2	2279	145	2293	241	0.82	0.17
2% NO/98% H_2	2450	168	2467	279	0.95	0.21
1% NO/99% H_2	2598	179	2616	297	1.07	0.24

collision-induced vibrational $v = 0 \rightarrow 1$ excitation. This background is corrected for by the subtraction of reference spectra recorded with the IR laser blocked.

To generate molecular beams of NO with different translational energies, we mixed NO with different carrier gases (H_2 and N_2) in various concentrations (see Table I, which gives each beam's translational energy distribution). For every gas mixture, the NO translational energy distribution was measured as described previously.[30]

Angular distributions of scattered NO molecules were measured by translating the unfocused REMPI laser along a line perpendicular to the incident molecular beam, and recording the signal for a given transition (corresponding to a certain v, J state) as a function of the laser beam position. Because this method always probes a cylindrical volume along the laser beam, the measured angular distributions will appear narrower than they would with a point detector. These experimental effects and how to handle them have been reported in detail elsewhere; they are only significant for relatively broad angular distributions.[23]

B. Theory

The IESH calculations were performed with the same code, potential energy surface, and nonadiabatic coupling used previously for NO/Au(111) vibrational relaxation[22] and excitation.[26] This approach, which is an extension to the original surface hopping scheme,[19] is explained in detail in Refs. 20 and 21. Briefly, the molecule-surface interaction is described by a many-electron Newns-Anderson Hamiltonian.[31,32] The metal continuum is modeled as a set of M_s discrete states populated with the appropriate number of electrons, $N_e = M_s/2$. The interaction of neutral and ionic states of the NO molecule with the surface as well as the nonadiabatic coupling functions were determined by fitting physically reasonable pair potentials to the results of DFT calculations performed for different NO positions and orientations relative to the surface.[20] We used the same potential energy surfaces and nonadiabatic couplings as in previous IESH studies for NO/Au(111).[22,25,26] For comparison, analogous simulations were performed using an adiabatic model, employing the same code as for the IESH simulations but suppressing the electronic surface hopping. We also made comparison to an implementation of EF theory,[33] using the same potential energy surface as for the IESH calculations. As the molecular vibration is treated classically in these models, a quantum-classical correspondence rule has to be applied in order to assign vibrational quantum numbers. We used the Bohr-Sommerfeld quantization rule[34] to calculate the classical action as a function of molecular rotational and vibrational energy and simple box binning for the quantization, as described previously.[25]

Our implementation uses $M_s = 80$ discrete energy levels populated by $N_e = 40$ electrons to represent the electronic continuum of the metal. The time step for the numerical integration of the equations of motion was set to $\Delta t = 0.1$ fs. For each incidence energy of translation, we simulated 1000 trajectories. The initial vibrational energy was set to $E^0_{\text{vib}} = 0.80$ eV, corresponding to vibrational state $v = 3$, with the harmonic vibrational frequency of NO in its X $^2\Pi$ ground state equal to $\omega_e = 1904.2$ cm^{-1}. The initial rotational energy was set to $E^0_{\text{rot}} = 0$; the initial positions and orientations of the NO molecule were chosen randomly. Simulations were performed for incidence translational energies, E_i, ranging from 0.1 eV to 1.2 eV. If after 20 ps simulation time the molecule was still within 10 Å from the top Au atom layer, the molecule was considered as trapped on the surface, and the trajectory was excluded from all further analysis.

For each remaining trajectory, we determine the number of bounces that the molecule experiences during its collision with the surface with the following procedure. From the N and O atom coordinates and velocities, which were saved at every 10th time step, i.e., for every fs, we extract the center-of-mass acceleration of the molecule as a function of time. The resulting curve is smoothed using a moving average with a width of 17.5 fs, corresponding to one vibrational period, in order to remove the fast oscillations originating from the classical molecular vibration. We then count how many times the z-component of the center-of-mass acceleration exceeds a certain fraction (1/8) of its maximum along the trajectory for a certain minimum time (1 fs), and define this as the number of bounces, b. This information is condensed by classifying the trajectories as single ($b = 1$), double ($b = 2$), or multiple ($b > 2$) bounce events.

We are aware that our definition of a bounce is not the only possible one. In particular, one could count a bounce whenever the z-component of the center-of-mass velocity, v_z, changes sign, or one could apply our algorithm using the norm

of the acceleration, $|a|$, instead of its z-component, a_z. Similarly, one could choose different parameters for the acceleration threshold and minimum bounce duration. We carefully examined several algorithms and found that they yield only slightly different results. Our choice is based on the following arguments: (1) Looking only at sign changes of v_z misses collisions that considerably slow down the center of mass but do not reverse it, such as when the O atom first collides with the repulsive potential but the N atom continues moving into the surface. (2) Using $|a|$ instead of a_z has the advantage that it is sensitive to bounces in x and y directions, but has the disadvantage that multiple bounces are often counted as one because $|a|$ does not fall below the threshold between the bounces, probably due to lateral or attractive forces. (3) The choice of threshold was made by manual inspection of several trajectories. It turned out that a constant threshold is not a reasonable choice over the broad range of incidence energies because molecules with low incidence energy typically experience much lower acceleration. In summary, we tested several possible algorithms and chose one that appears to produce the most physically reasonable results.

III. RESULTS

A. REMPI spectra

Representative REMPI spectra of scattered NO molecules recorded at four different translational incidence energies are shown in Figure 1. The population of NO in vibrational states $v = 1,\ 2,\ 3$ is probed via the A $\leftarrow$ X 0–1, 0–2, and 1–3 bands near 236 nm, 247 nm, and 244 nm. The spectra were corrected for laser power, detector gain, and Franck-Condon factors.[35] The three bands are clearly separated except for a small overlap between the 1–3 and 0–2 bands, which is significant only at higher incidence energies, where stronger rotational excitation is observed. This spectral overlap was taken into account in our data analysis; see Sec. III B. A cursory inspection of the REMPI spectra shows that the branching ratio between vibrational relaxation into $v = 2, 1$ and survival in $v = 3$ changes with incidence energy. The data clearly indicate that as the incidence energy is increased, the integrated intensities of the 0–2 and 0–1 bands grow at the expense of the 1–3 band intensity.

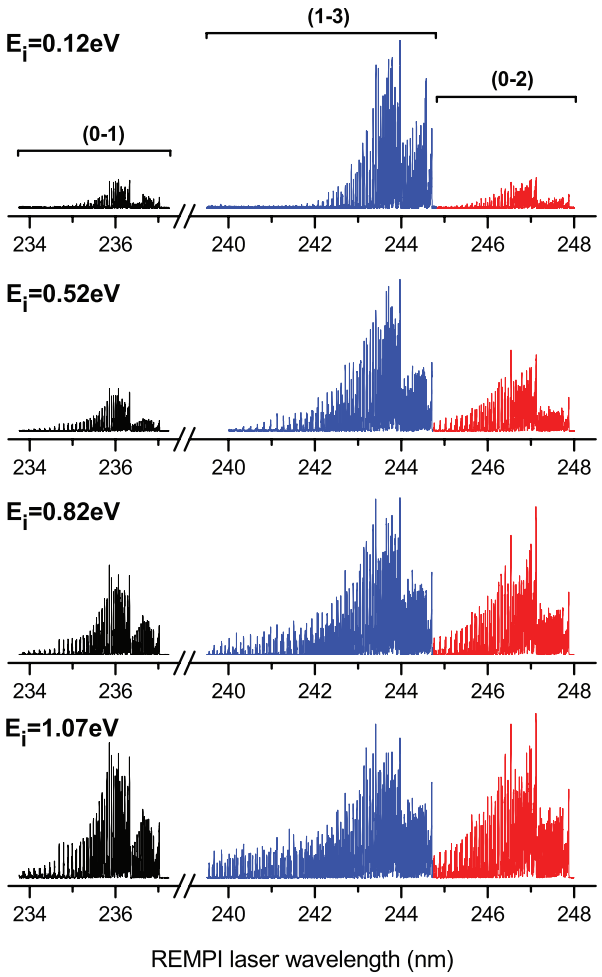

FIG. 1. REMPI spectra, corrected for laser power, detector gain, and Franck-Condon factors, recorded at four different incidence energies. The 0–1, 0–2, and 1–3 bands probe the populations of $v = 1,\ 2$, and 3 after the scattering process, respectively. For each incidence energy, the three bands are shown on the same scale, illustrating the relative branching. The vertical scales for the different incidence energies were adjusted for optimum visibility. As the incidence energy is increased, the $v = 1$ and $v = 2$ populations grow at the expense of the $v = 3$ population.

B. Extraction of branching ratios

Obtaining the absolute vibrational relaxation probabilities is complicated since the $v = 3 \rightarrow 0$ channel is practically impossible to observe due to the NO($v = 0$) background in the incident beam. All measurements were thus normalized to the sum of the signals for elastically scattered $v = 3$ and de-excited $v = 2$ and $v = 1$, i.e., we calculate the branching ratios

$$R(v) = S(v)/[S(1) + S(2) + S(3)], \qquad (1)$$

where $S(v)$ is the integrated signal strength for a given vibrational state.

The signal strengths, $S(v)$, were obtained by integrating the individual vibrational bands 0–1, 0–2, and 1–3 in the REMPI spectra, after correcting the raw data for laser power, detector gain, temporal dilution, and Franck-Condon factors as explained in detail in a previous publication.[23] In addition, the effects of slightly different vibration-to-translation coupling for the three channels were taken into account.[30] The small overlap between the 0–2 and 1–3 bands was accounted for by measuring an additional 0–2 spectrum at high surface temperature ($T_S = 900$ K) without the IR beam. In this scan we mainly observe the $v = 0 \rightarrow 2$ excitation while $0 \rightarrow 3$ excitation is negligible.[25] Assuming that the rotational distribution is independent of T_S and Δv, which is a good assumption,[23] we determine the fraction of the 0–2 band that is overlapped with the 1–3 band. In all further analysis, this correction is applied to the $v = 2$ and $v = 3$ signals.

The branching ratios constitute upper limits to the true probabilities, $P(v) = S(v)/\sum_w S(w)$, where w runs over

all vibrational states. Significant additional contributions are only expected from $S(0)$ and $S(4)$. We expect the latter to be smaller than $S(3)$ by at least two orders of magnitude, judging from the measured $v = 0 \rightarrow 1$ vibrational excitation probabilities, which at $T_S = 300$ K are $<10^{-3}$ even at the highest incidence energies.[26] Regarding the contribution of $S(0)$, no experimental data are available, however the evaluation of single-bounce IESH trajectories suggests that $S(0)$ is small, see Sec. IV B.

C. Angular distributions

Before presenting the vibrational branching ratios, we point out that the angular distributions of scattered NO molecules are narrow for all detected vibrational states. As an example, we present the angular distributions for NO molecules scattered into $v = 1$, 2, and 3 at an incidence energy of $E_i = 0.52$ eV in Figure 2. We find that the distributions are quasi-specular and quite narrow with FWHM $\approx 44^\circ$. Fitting to $\cos^m(\theta - \theta_0)$ functions yields exponents $m = 8.8$–9.5.

The observation of narrow angular distributions is a clear indication that most molecule-surface collisions proceed as direct scattering rather than trapping and desorption, which would yield broad, $\cos\theta$, angular distributions.[36] This picture is corroborated by previously observed narrow angular distributions for NO($v = 0 \rightarrow 1$, 2, 3)/Au(111) scattering over a broad range of incidence energies;[23,25] final rotational distributions that depend strongly on incidence energy but only weakly on surface temperature, with rotational temperatures different from surface temperatures for NO($v = 0$)/Ag(111) and NO($v = 0 \rightarrow 1$, 2, 3)/Au(111) scattering;[23,37] and by clearly non-thermal recoil translational energy distributions for NO($v = 3 \rightarrow 3$, 2, 1)/Au(111) scattering.[30]

For incidence energies below 0.2–0.3 eV, it is known that trapping becomes significant for NO($v = 0$, 2)/Au(111), with experimentally determined trapping probabilities of approximately 0.05 at $E_i = 0.3$ eV, 0.15 at $E_i = 0.2$ eV, and 0.38 at $E_i = 0.1$ eV.[38] As the trapping probabilities were found to be insensitive to the initial vibrational state, we may assume that similar numbers apply to NO($v = 3$) scattering. We conclude that at low incidence energies below approximately 0.3 eV, there is a fraction of molecules that undergoes trapping-and-desorption. We assume that any trapped NO($v = 3$) molecules remain on the surface long enough to be fully relaxed to NO($v = 0$), which we cannot detect even after prompt desorption.

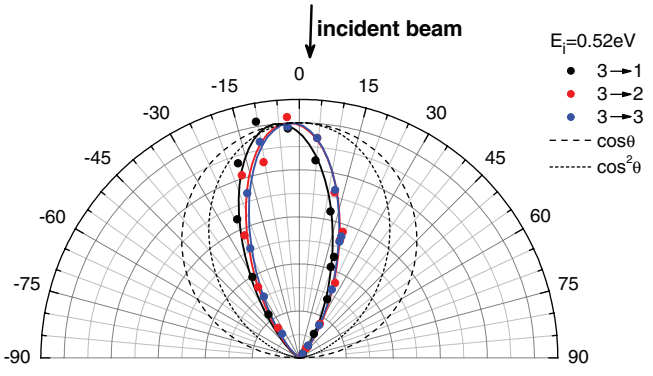

FIG. 2. Experimentally observed angular distributions for vibrational channels $3 \rightarrow 1$, 2, 3 recorded at an incidence energy of $E_i = 0.52$ eV. The solid lines are $\cos^m(\theta - \theta_0)$ fits to the experimental data, with exponents $m = 8.8$–9.5. The dashed lines are $\cos\theta$ and $\cos^2\theta$ distributions, the two limiting cases of angular distributions expected for a trapping-desorption mechanism under our conditions.[23] The observation of narrow angular distributions indicates that the collisions happen in a direct single-bounce mechanism.

D. Branching ratios

Experimental branching ratios as a function of incidence energy, $R(1)$, $R(2)$, and $R(3)$, are extracted from the REMPI spectra as discussed above and are shown in Figure 3 (left panel, black solid lines). We find that the branching ratios for vibrational relaxation $R(1)$, $R(2)$ increase with incidence energy while the branching ratio for vibrationally elastic scattering $R(3)$ decreases with incidence energy.

These observations agree qualitatively with the earlier experimental results for NO($v = 2$) scattering from Au(111), which show that the probabilities for both vibrational excitation ($v = 2 \rightarrow 3$) and relaxation ($v = 2 \rightarrow 1$) increase with the translational incidence energy.[27] Assuming that both relaxation to $v = 0$ and trapping are negligible, our definition of $R(3)$ is in complete analogy with the $v = 2$ vibrational survival probability, NO($v = 2$)/[NO($v = 1$) + NO($v = 2$)], as defined in Ref. 27. A direct comparison is presented in Figure 3 (gray dashed line). Our $v = 3$ survival probabilities are found to be consistently and significantly smaller than the previously measured $v = 2$ survival probabilities. We speculate that the corresponding enhanced relaxation from $v = 3$ as compared to $v = 2$ could be due to the stronger intrinsic coupling for higher vibrational states, specifically the rate for $3 \rightarrow 2$ relaxation is expected to be higher than the rate for $2 \rightarrow 1$ relaxation by a factor of 3/2.[18] However, more detailed experimental studies are needed for a definite answer.

E. Theoretical simulations

For comparison, we calculated the vibrational branching ratios using the IESH model. A comparison between the experimental and theoretical results is presented in Figure 3 (left panel, red dashed line). The IESH model predicts strong relaxation into $v = 2$ and 1. Not visible from the branching ratios, a significant fraction of trajectories (up to 40% at $E_i = 0.1$ eV) is found to fully relax to $v = 0$, as shown in the inset diagram of Figure 3. Because the experiments cannot probe scattering into $v = 0$, we calculate the $v = 1$, 2, 3 branching ratios using IESH according to Eq. (1) as we have done for the experimental data.

From Figure 3 (left panel) it is clear that molecular dynamics with IESH predicts an incidence energy dependence counter to what we find in experiment, namely, increasing relaxation for smaller incidence energy. This is quite a dramatic disagreement. In principle such problems could arise

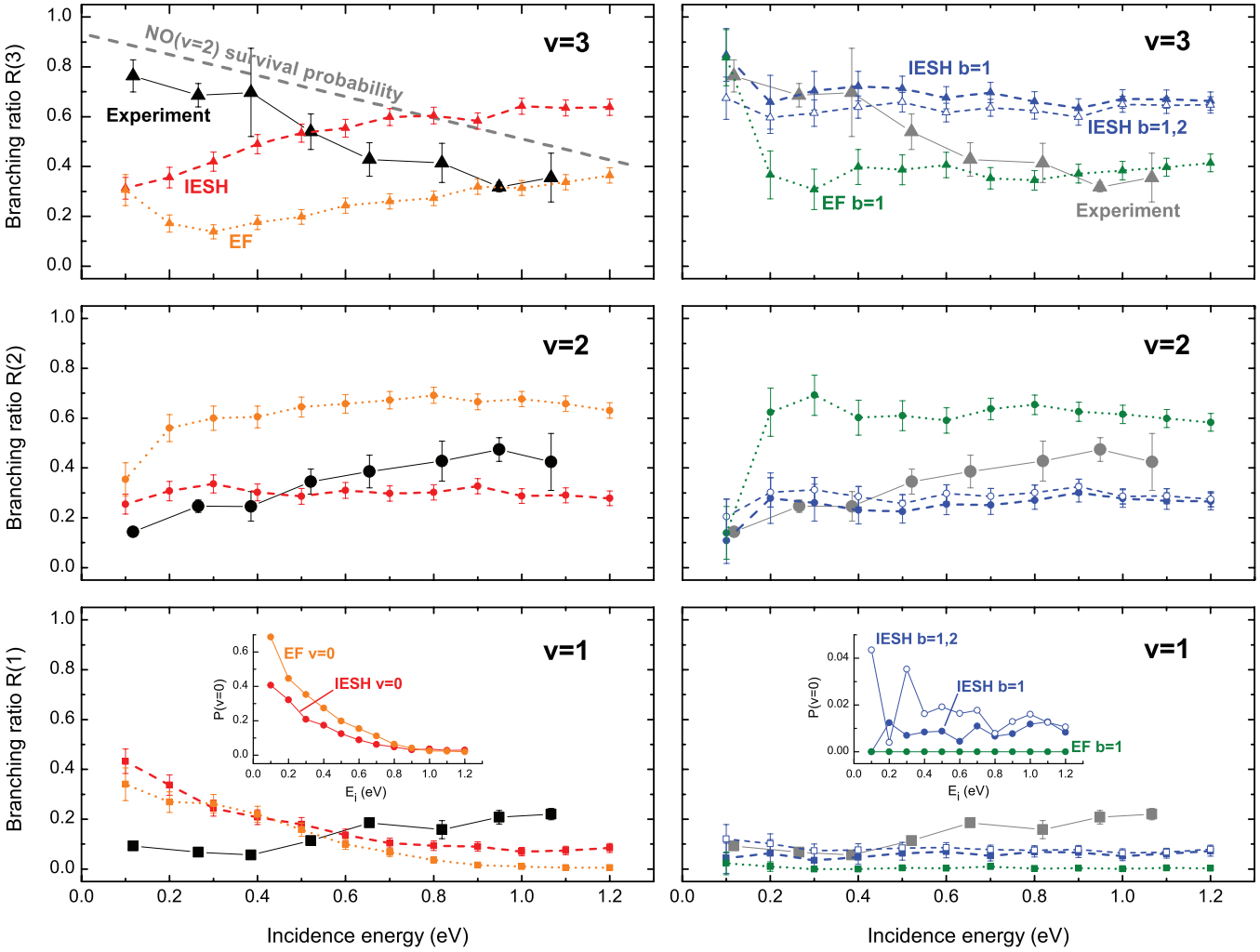

FIG. 3. Branching ratios $R(v)$ for scattering into vibrational states $v = 1,\ 2,\ 3$. The left panel shows a comparison of experimental data (black symbols, solid line) to the results of IESH (red, dashed) and EF calculations (orange, dotted) when we analyze all trajectories. For comparison, the NO($v = 2$) survival probability from Ref. 27 is also shown in the R(3) panel (gray dashed line). The right panel shows the IESH (blue, dashed) and EF (green, dotted) results when the analysis is restricted to trajectories with a single bounce ($b = 1$), compared to the same experimental data. In addition, the right panel shows IESH results for a restriction to trajectories with a single or double bounce ($b = 1, 2$; open symbols). The inset diagrams show the calculated absolute probabilities for complete relaxation to $v = 0$. The error bars on the experimental data indicate statistical uncertainties originating from pulse energy fluctuations of the IR and UV lasers; the error bars on the simulation data represent 2σ (95% confidence) statistical uncertainty. Experimentally we find that vibrational relaxation increases with incidence energy at the expense of vibrationally elastic collisions. IESH predicts the wrong dependence on incidence energy, but the restriction to single-bounce trajectories attenuates this trend and yields better agreement with the experimental results. The restriction to single or double-bounce trajectories has a similar but slightly weaker effect. EF predicts much stronger vibrational relaxation from $v = 3$, and it also exhibits the wrong dependence on incidence energy except at the lowest values. For EF, the selection of single-bounce trajectories also has a strong influence on the E_i dependence. But the most drastic change is that after selection of single-bounce trajectories, relaxation by more than one vibrational quantum, i.e., $v = 3 \rightarrow 1, 0$, is essentially suppressed.

from two sources, either from errors introduced by the surface hopping dynamics or from errors in the *ab initio* input data (interaction potential and nonadiabatic couplings) required to carry out the IESH calculation. In Secs. IV A–IV C we present evidence of our conclusion that it is principally the *ab initio* input data that lead to the disagreement between experiment and theory.

We also performed simulations of the vibrational branching ratios using an EF model. It predicts significantly stronger vibrational relaxation than IESH for all but the lowest incidence energies. For $E_i > 0.3$ eV, it also shows increasing relaxation for smaller E_i. Compared to IESH, there is considerably more one-quantum relaxation into $v = 2$. We will return to a discussion of the differences between EF and IESH later in the paper.

IV. DISCUSSION

A. Multiple bounces analysis

As explained above, our implementation of molecular dynamics with IESH predicts that vibrational relaxation decreases with incidence energy and thus fails to reproduce the experimental observations (Figure 3). We will now show that this failure of the simulations is related to the number of bounces that a molecule experiences as it collides with the surface. For this purpose, we extracted the number of bounces, b, for a series of incidence energies, as described in Sec. II B. Typical trajectories representative for collisions with one, two, and many bounces are shown in Figure 4.

For a more quantitative and detailed view, we show the fractions of single-bounce ($b = 1$), double-bounce

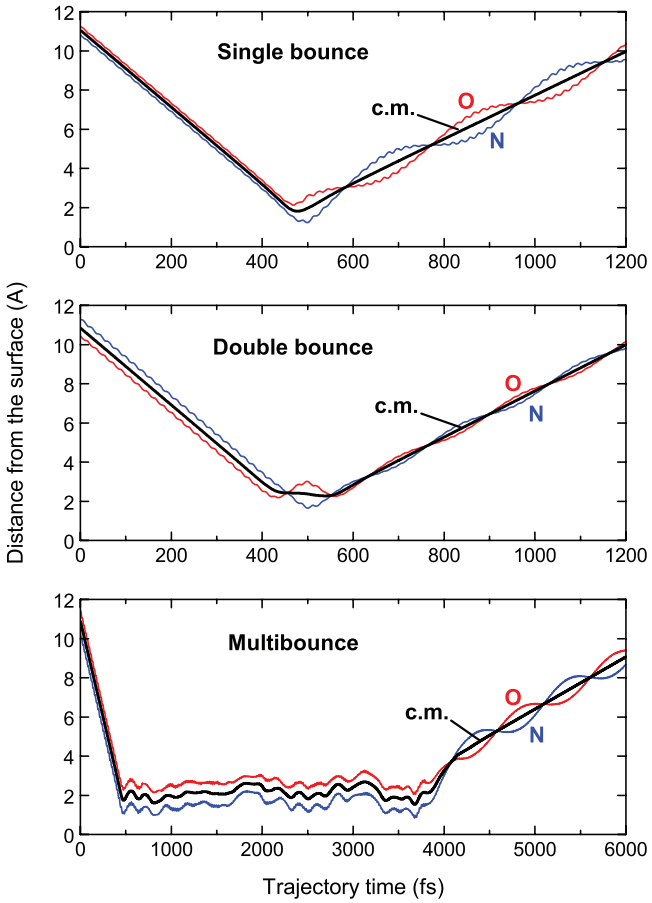

FIG. 4. Typical IESH trajectories for molecule-surface collisions with a single, double, and multiple bounces. The translational incidence energy is 0.6 eV in all cases. The blue and red lines show the N and O atom distance from the surface (z coordinate) as a function of trajectory time. The thick black line shows the corresponding curve for the center of mass of the NO molecule. Looking closely one sees that the single bounce happens for an N-down collision, while the double bounce happens for an O-down collision. For the single bounce, the molecule is still vibrating as it leaves the surface, whereas for the multi-bounce collision it loses most of its vibrational energy. Molecular rotation is excited in all three cases. These observations of course depend on the individual trajectories, but the behavior shown here is quite typical.

($b = 2$), and multiple-bounce ($b > 2$) trajectories as a function of incidence energy in Figure 5 (solid symbols). We observe that the fraction of single-bounce collisions increases with incidence energy from only ≈5% at $E_i = 0.1$ eV to >70% at 1.2 eV. The fraction of multiple-bounce collisions shows the opposite trend, decreasing from ≈85% at $E_i = 0.1$ eV to only ≈6% at $E_i = 1.2$ eV. The fraction of double-bounce collisions varies from ≈10% at $E_i = 0.1$ eV to ≈23% at $E_i = 1.2$ eV, with a maximum of ≈30% near $E_i = 0.7$ eV. Clearly the average number of bounces is higher for lower incidence energies.

One might think that these low probabilities for single-bounce collisions result from nonadiabatic interaction of the NO molecule with the solid. Both IESH and EF open an additional channel for the conversion of energy from nuclear to electronic degrees of freedom, which could help to efficiently remove translational energy—a prerequisite for trapping the molecule on the surface. However, we observe quite similar behavior for calculations using the IESH, adiabatic or EF

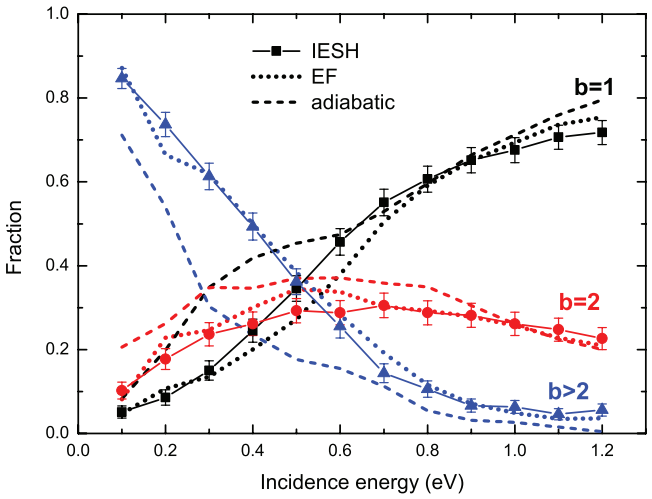

FIG. 5. Fractions of trajectories with $b = 1$, $b = 2$, or $b > 2$ bounces, as a function of incidence energy, for IESH (solid line with symbols), EF (dotted), and adiabatic (dashed) simulations. We find that the fraction of multi-bounce trajectories drastically increases for lower incidence energies. This behavior is somewhat more pronounced for IESH and EF than for adiabatic simulations, but the general trend is similar for all three models.

models; see Figure 5. Although the fraction of multi-bounce trajectories is slightly lower for the adiabatic model than for IESH or EF, it still reaches more than 70% at $E_i = 0.1$ eV, and the trend is the same as for IESH. This indicates that the surface hopping scheme is only partially responsible for the high fraction of multi-bounce collisions at low incidence energy and that a more accurate treatment of the adiabatic translational inelasticity could dramatically change this behavior.

Based on the clear experimental evidence that most collisions happen in a direct single-bounce regime, the results of Figure 5 represent a qualitative failure of our implementation of molecular dynamics with IESH. Although it is a quite challenging undertaking to revise the theoretical model so that it more accurately reproduces the single-bounce nature of the scattering, it is interesting to investigate how the present results depend on the number of bounces. We use this approach for the current discussion, but we do not claim that it is equivalent to a modified theoretical model that avoids multi-bounce collisions from the beginning.

B. Branching ratios after selection of single-bounce trajectories

Surface collision induced vibrational relaxation energy distributions, calculated using IESH and EF for a representative incidence translational energy, $E_i = 0.4$ eV, show that the degree of vibrational relaxation is quite different for trajectories with one, two, or more bounces—the strongest vibrational relaxation is observed for multi-bounce trajectories (see Appendix A for details, Figure 9). As the typical number of bounces depends strongly on incidence energy, as shown in Figure 5, it is to be expected that the selection of single-bounce trajectories has the strongest effects on the predicted vibrational energy distribution for the lowest incidence energies.

In order to test this hypothesis, we repeated the analysis for the subsets of IESH trajectories with $b = 1$ (single bounce) and $b = 1, 2$ (single or double bounce). These results are color-coded blue in Figure 3 (right panel). We carried out the same analysis for EF dynamics, results which are color-coded green in Figure 3 (right panel). While the single-bounce results are similar to the all-trajectories IESH results at high incidence energies, where the fraction of single-bounce collisions is high, they clearly deviate at lower incidence energies. In fact, the predicted dependence on incidence energy is now much weaker: The single-bounce relaxation probabilities are almost independent of incidence energy. The selection of single-bounce trajectories brings the incidence energy dependence into better agreement with the experimental data, but the experimentally observed incidence energy dependence is still not quantitatively reproduced.

A closer look at the trajectories shown in Figure 4 reveals that the single-bounce collision happens as the molecule approaches the surface with its N atom first while the double-bounce collision happens when the molecule collides with its O atom first. This observation is quite representative, and one could argue that the selection of single-bounce trajectories preferentially selects N-down collisions, and that selecting all trajectories that exhibit a single *or* a double bounce would also be a reasonable restriction. The corresponding branching ratios for $b = 1, 2$ are also shown in Figure 3 (right panel, open symbols). In general, they are very similar to those obtained for single-bounce selection. However, it appears that the selection of single or double-bounce trajectories has a slightly weaker effect than the selection of only single-bounce trajectories.

Not surprisingly, the selection of single-bounce trajectories also strongly reduces the complete relaxation to $v = 0$ (Figure 3, right panel inset). We find probabilities as small as $\approx$0.01 over the full range of incidence energies. Judging from the overall improved agreement of single-bounce IESH with experimental data, we tend to trust the single-bounce IESH results for $v = 0$ as well. If such trust were justified, the branching ratios as defined in Eq. (1) would become essentially equivalent with absolute probabilities.

For the EF simulations, the selection of single-bounce trajectories has the strongest effect on the $v = 1$ branching ratio, which becomes negligible over the full range of incidence energies. Relaxation to $v = 0$ is completely suppressed (inset diagram). The wrong incidence energy dependence of $R(3)$ becomes less pronounced and the agreement with the experimental data is thus improved, similar to what we find for IESH. However, EF overestimates the $R(2)$ branching ratio while at the same time it drastically underestimates the $R(1)$ branching ratio. This clearly shows that multi-quantum vibrational relaxation appears in the EF model only when unphysical multi-bounce collisions are present. While our IESH simulation also exhibits these multibounce artifacts, when we select for single bounce collisions only, we obtain reasonable agreement for $R(2)$ and $R(1)$ over the entire range of translational incidence energies. This indicates that a strong coupling model, where energy is exchanged between nuclear and electronic degrees of freedom in more than infinitesimal amounts – as implemented in IESH but not in EF – is essential for a correct description of the NO/Au(111) vibrational relaxation dynamics.

Before we move on, we point out that the comparison of IESH to experimental results in our previous study of NO/Au(111) vibrational *excitation* – despite good overall agreement – revealed some minor discrepancies.[26] In particular, the incidence energy dependence of the vibrational excitation probabilities is not correctly captured by the IESH simulation, which predicts constant or even slightly decreasing probabilities over the investigated range of incidence energies. It seems reasonable to hypothesize that this disagreement may have the same origin as we find here for relaxation. This could be tested by evaluating the IESH results for vibrational excitation only for single-bounce collisions, analogous to this study, but would require a significantly larger number of trajectories in order to predict the small excitation probabilities $[P(v = 1) = 3 \times 10^{-4} \ldots 2 \times 10^{-2}$; $P(v = 2) = 1 \times 10^{-5} \ldots 6 \times 10^{-4}]$ with sufficient statistics.

C. Origins of the discrepancy between theory and experiment

We will now analyze the theoretical results in more detail in order to show what causes the wrong incidence energy dependence of vibrational relaxation, and ultimately be able to make suggestions how to improve the model. In IESH, the vibrational relaxation is dominated by the nonadiabatic coupling of nuclear and electronic degrees of freedom, which is implemented following the surface hopping scheme.[19,39] At every time step, the electrons may hop from one adiabatic potential energy surface to another, with the probabilities for such hops governed by the nonadiabatic coupling vector.

We evaluated the average number of electronic hops per trajectory, $\langle H \rangle$, first for all trajectories and then separately for the subsets of trajectories with 1, 2, and >2 bounces. The results are shown in Figure 6. We observe that for the analysis of all trajectories, the average number of electronic hops increases drastically as the incidence energy is decreased, from $\langle H \rangle \approx 11$ at $E_i = 1.2$ eV to $\langle H \rangle > 100$ at $E_i = 0.1$ eV. The detailed analysis however shows that for single and double-bounce trajectories, the average number of electronic hops is $\langle H \rangle < 10$ at any incidence energy, and at least for single-bounce trajectories it actually decreases at low incidence energies. For collisions with more than two bounces, the average number of hops is much higher, $\langle H \rangle \approx 100$, over the full range of incidence energies, slightly increasing at low incidence energy and reaching $\langle H \rangle \approx 150$ at $E_i = 0.1$ eV.

One could speculate that every time the molecule bounces off the surface, it has a certain chance to execute an electronic hop and that not all bounces have the same chance. Clearly for individual bounces, the hopping probabilities will depend on the exact coordinates, such as the depth of the penetration, the impact position on the (111) surface lattice, and the molecular orientation. This will be considered in more detail below. But in general we conclude that the more bounces the molecule experiences, the more electronic hops will happen.

It is interesting that only by restricting the analysis to single-bounce trajectories, we find the expected trend that

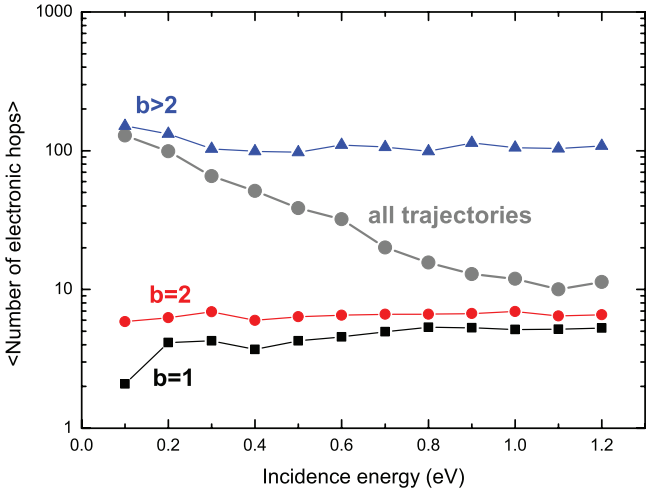

FIG. 6. The average numbers of electronic hops, evaluated for all trajectories (big gray circles) and selectively for single-bounce (black squares), double-bounce (red circles), and multiple-bounce (blue triangles) trajectories. Analyzing all trajectories, we find that the average number of hops drastically increases as the incidence energy is decreased (note the log scale). The detailed analysis shows that the average number of hops is always much higher for multi-bounce than for single and double-bounce trajectories, and that its increase at low E_i is probably due to the increasing fraction of multi-bounce trajectories.

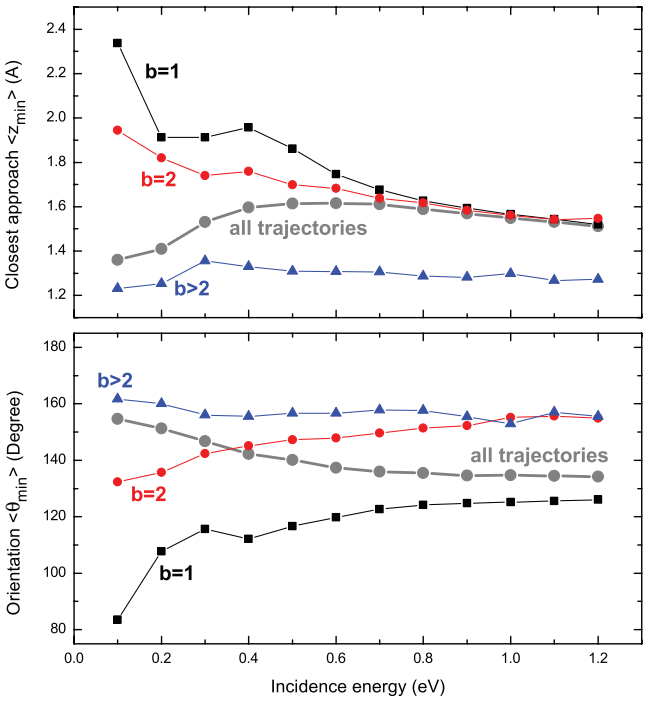

FIG. 7. Coordinates at closest approach, evaluated for all (big gray circles), single (black squares), double (red circles), and multiple (blue triangles) bounce trajectories. Top panel: The average minimal z value, $\langle z_{\min}\rangle$. Bottom panel: The average angle of the internuclear axis (O → N) with the z-axis at the instant of closest approach, $\langle\theta_{\min}\rangle$, where 0°, 180° correspond to perfect O, N down orientation. For single and double-bounce trajectories, $\langle z_{\min}\rangle$ decreases as the incidence energy is increased, in accordance with expectation. For multi-bounce trajectories, $\langle z_{\min}\rangle$ is nearly constant, and very small. The overall trend mostly results from the changing fractions of single, double, and multi-bounce trajectories. Similar conclusions apply for the orientation at closest approach, where favored N-down orientation with $\langle\theta_{\min}\rangle$ near 160° is found for multi-bounce trajectories over the full range of incidence energies.

$\langle H\rangle$ increases with incidence energy. Nevertheless, even here this trend is weak. The increase of the $\langle H\rangle$ curve for $b > 2$ collisions at low E_i is likely due to the increasing average number of bounces. The results suggest that the increasing numbers of electronic hops at low incidence energies are entirely caused by the increasing fraction of multi-bounce trajectories.

Finally, we focus on the coordinates and the orientation of the NO molecule at the instant of its closest approach to the surface. In the simulation, the z-axis is chosen perpendicular to the metal surface, with $z = 0$ defined by the centers of the gold atoms in the top atomic layer, at their equilibrium positions. For every trajectory, we record the closest approach, $z_{\min}$, defined as the minimal z coordinate of either the N or O atom, whichever is smaller. We also record the angle of the NO internuclear axis with the z-axis, $\theta_{\min}$, at the instant when $z_{\min}$ is achieved. The definition is such that $\theta_{\min} = 0$ and $\theta_{\min} = 180°$ correspond to perfect O-down and N-down orientations of the NO molecule, respectively. The nonadiabatic interaction is strongest for closest approach to the surface, i.e., for small values of $z_{\min}$, and for strong N-down orientation of the molecule, i.e., values of $\theta_{\min}$ approaching 180°.[22]

The calculated mean values $\langle z_{\min}\rangle$ and $\langle\theta_{\min}\rangle$ as a function of incidence energy are shown in Figure 7. We find that for the full set of trajectories, the "best" coordinates for strong interaction, small $\langle z_{\min}\rangle$ and $\langle\theta_{\min}\rangle$ near 180°, are assumed at the smallest incidence energy, $E_i = 0.1$ eV. However, the separate analysis of trajectories with 1, 2, and >2 bounces shows that again this results from the gradually increasing fraction of multi-bounce trajectories as the incidence energy is decreased.

For single and double-bounce trajectories, $\langle z_{\min}\rangle$ becomes smaller with increasing incidence energy, in accordance with expectations. For multi-bounce trajectories, small $\langle z_{\min}\rangle$ values are assumed over the full range of incidence energies, but their influence is significant only at low E_i where the fraction of multi-bounce trajectories is high. Regarding the molecular orientation θ, which initially follows a $\sin\theta$ distribution, we find that $\langle\theta_{\min}\rangle$ increases with incidence energy from near 90° to ≈125° for single-bounce trajectories, whereas it is constant near $\langle\theta_{\min}\rangle \approx 160°$ over the whole range of incidence energies for multi-bounce trajectories. For double-bounce trajectories, the behavior is intermediate between the single and multiple bounce cases. The observed $\langle\theta_{\min}\rangle$ increase with incidence energy for single and double-bounce collisions is probably related to the associated closer approach to the surface, where the interaction potential exerts a stronger torque toward N-down orientation.

It is well known from many experiments that the nonadiabatic coupling, which is the origin of vibrational excitation and relaxation during NO/Au collisions, increases with incidence energy.[23,26] The present implementation of molecular dynamics with IESH, considering all trajectories, predicts that the distance of closest approach $\langle z_{\min}\rangle$ and the corresponding molecular orientation $\langle\theta_{\min}\rangle$ are nearly independent of incidence energy, or even exhibit the wrong incidence energy

dependence. When we consider only the single-bounce collisions, we find that the $\langle z_{min}\rangle$ and $\langle \theta_{min}\rangle$ expectation values exhibit the correct incidence energy dependence. This observation clearly suggests that an improved model, which succeeds in eliminating this multi-bounce artifact, will be able to better reproduce the dependence of vibrational excitation and relaxation rates on the incidence translational energy.

A more detailed analysis of the z_{min} distributions shows that for incidence energies below ≈0.4 eV, the z_{min} distribution develops an extra peak at very small values, $z_{min} \leq 1.2$ Å, which is exclusively caused by multi-bounce trajectories (see Appendix B, Figure 11). Analogous but less pronounced behavior is found for the θ_{min} angles, which assume the largest values near 180° (N-down) mostly during multi-bounce collisions. Apparently, the z_{min} and θ_{min} coordinates are more favorable for strong nonadiabatic interaction for multi-bounce than for single-bounce collisions.

A simple picture emerges from the observations presented above. Namely, they suggest that the molecule is steered towards the optimum geometry for nonadiabatic energy exchange as a result of the multi-bounce encounter with the surface. In order to test this more carefully, we recorded the closest approach and corresponding orientation during every individual bounce, $z_{min}^{(j)}$ and $\theta_{min}^{(j)}$, where j ($j = 1, 2, 3\ldots$) designates the first, second, third bounce, and so on. For trajectories with more than two bounces, we define $z_{min}^{(>2)}$ as the minimal value of all $\{z_{min}^{(j)}; j > 2\}$, and $\theta_{min}^{(>2)}$ as the corresponding $\theta_{min}^{(j)}$ value. Note that this analysis was restricted to trajectories with at least three bounces.

The resulting distributions for the $z_{min}^{(1,2,>2)}$ and $\theta_{min}^{(1,2,>2)}$ values assumed during the first, second, and any later bounces, for $E_i = 0.1$ eV, are shown in Figure 8. We picked the lowest incidence energy, where the fraction of multi-bounce trajectories is the highest, in order to get good statistics. The results confirm that with each additional bounce the NO molecule is steered to a more favorable geometry for energy exchange. This is most important at low incidence energies of translation. The smallest z_{min} values, especially those with $z_{min} < 1.2$ Å, are rarely assumed during the first or second bounce, but mostly during later bounces of a molecule with the surface. In analogy, the most favorable orientations, i.e., θ_{min} values near 180°, are mostly assumed during later-than-second bounces. We suppose that while the molecule is near the surface, it is driven toward the favored geometry for strong nonadiabatic interaction by the specific forces of the Au-N and Au-O interaction potentials. This argument is consistent with the previously suggested dynamical steering,[22] but in this case would also apply to a molecule that is temporarily trapped on the surface.

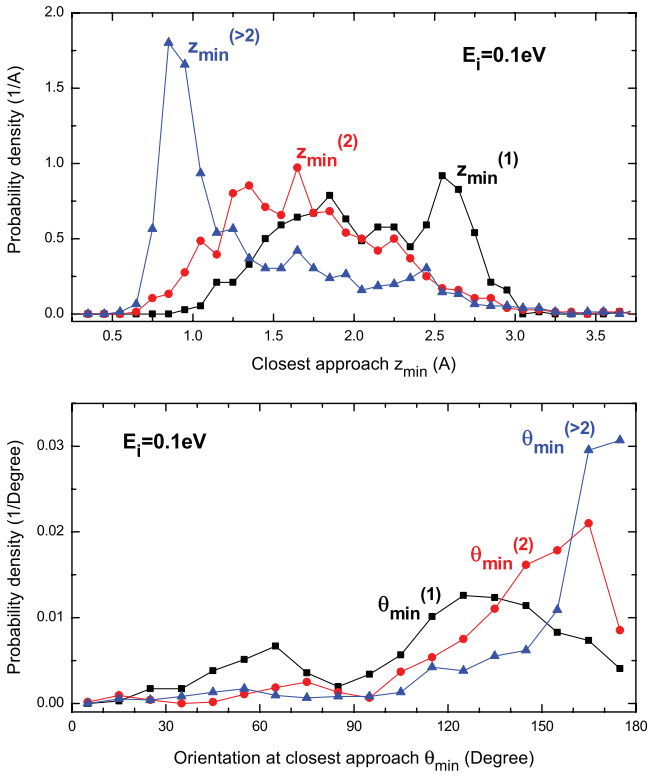

FIG. 8. Distributions for $z_{min}^{(j)}$ (top) and $\theta_{min}^{(j)}$ (bottom), i.e., the z_{min} and θ_{min} values assumed during the jth bounce, for incidence energy $E_i = 0.1$ eV. The values for $z_{min}^{(>2)}$ and $\theta_{min}^{(>2)}$ indicate the minimal z_{min} value assumed during any later-than-second bounce, and the corresponding orientation. The distributions show that the favored geometries, small z_{min} and θ_{min} near 180°, are preferentially assumed during later bounces. Only trajectories with more than two bounces were considered for this analysis.

D. Suggestions for improvements to the theoretical model

The detailed comparison of experimental data with simulations based on molecular dynamics with IESH revealed that the theoretical model in its current implementation fails to describe the incidence energy dependence for vibrational relaxation of NO($v = 3$). However, the incidence energy dependence is brought into better agreement with experimental data by selecting only those trajectories where the molecules undergo single-bounce collisions with the surface. The prediction of large fractions of multi-bounce collision trajectories at moderately low incidence energies (the fraction of multi-bounce trajectories exceeds 50% at incidence energies below ≈0.4 eV) is a fundamental failure of the current implementation. The fact that collisions with multiple bounces occur almost as frequently in an adiabatic model, as shown in Figure 5, suggests that the surface hopping scheme is not to blame.

Rather it suggests that the problem is with the present implementation of the multidimensional potential energy surface, i.e., the interaction of the NO molecule with the gold crystal as well as the interaction of the gold atoms in the crystal. From the high average numbers of bounces one could conclude that the surface is "too soft" in the sense that when the molecule collides with the surface, too much of its translational kinetic energy is converted into other degrees of freedom, allowing the molecule to temporarily be trapped on the surface. While the interaction of the N and O atoms with the Au surface is fit to the results of DFT calculations performed for many different geometries, the interaction between the Au atoms in the surface is not calculated from first principles but rather based on a Born-von Karman (empirical) force model.[20,40–43] In this model, the potential energy is described

as a harmonic function with interaction between nearest-neighbor gold atoms. It is conceivable that the observed deficiencies could be reduced by modification of the surface model. However, we point out that the current implementation is not arbitrary; the generalized force constants were obtained by fitting the calculated phonon dispersion spectrum to experimental data, and a good fit was obtained.[20] Obviously an improved model would still have to give good agreement regarding this comparison.

Another possible problem, which we consider more likely, is that the potential energy surface is too corrugated, such that – depending on the impact site – some artifactually large fraction of the normal component of incidence translational energy of the NO molecule would first be converted into motion parallel to the surface and later into other degrees of freedom. Such errors in the interaction potential could lead to enhanced multi-bounce encounters as only when the normal component of translational energy is high enough can a second bounce be avoided. This would implicate that the error is with the DFT calculations to which the potential energy surfaces are fitted. In order to improve the underlying calculations, one could consider to simply re-calculate DFT energies at a higher density of geometries or with a different choice of functional.

Such an approach may however be insufficient. It has been shown that electron transfer is an important part of the electronically nonadiabatic dynamics in this system.[26,44] It is believed that DFT may describe electron transfer inadequately in molecular interactions at metal surfaces.[45] Hence a more fundamental, but also more elaborate, improvement would be to replace the DFT calculation by more advanced methods such as quantum mechanical embedding theory, which allows a true *ab initio* description of the system.[46]

V. SUMMARY AND CONCLUSIONS

In summary, we have compared experimentally determined incidence-energy dependent vibrational relaxation branching ratios for NO($v = 3 \rightarrow 3, 2, 1$) scattering off a Au(111) surface to three different kinds of first-principles simulations: (1) adiabatic molecular dynamics, (2) molecular dynamics with electronic friction, and (3) molecular dynamics with independent electron surface hopping on a DFT derived Newns-Anderson Hamiltonian. All three approaches show serious disagreement with experiment. Methods (1) and (2) do not exhibit large enough vibrational relaxation probabilities and methods (2) and (3) exhibit a qualitatively incorrect dependence of relaxation probability on incidence energy, namely, they decrease with increasing incidence energy. The experimental data show that the relaxation probabilities increase with incidence energy, similar to previous measurements on NO($v = 2$) vibrational relaxation and NO($v = 0$) vibrational excitation.

All three simulations produce artificially high fractions of trajectories with multiple collisions rather than single-bounce scattering, especially at low incidence energies. A detailed analysis revealed that the multi-bounce collisions are associated with enhanced collision geometry, i.e., closer approach to the surface and near N-down collisions. Hence in IESH, this results in a higher average number of electronic hops and stronger nonadiabatic interaction. Removing all trajectories that are not classified as single-bounce collisions from the analysis, the incidence energy dependence is reversed, and the theoretical results exhibit improved agreement with experiment. While this is not a fix to the theory, it clearly suggests that a correct treatment of the translational inelasticity during the NO-Au collision is crucial for a correct description of nonadiabatic molecule-surface interaction, even though translational kinetic energy is not driving the vibrational transitions directly.

We also note that when we select only single-bounce trajectories, the EF model predicts $v = 3 \rightarrow 2$ to be the only significant relaxation channel, revealing a general shortcoming of EF, namely, its inability to describe direct multi-quantum (overtone) transitions. The EF model also appears to overestimate vibrational relaxation of $v = 3$ in comparison to IESH.

Finally, we wish to comment on previously published IESH calculations, which appear to successfully capture the multi-quantum vibrational relaxation of NO($v = 15$) colliding with a Au(111) surface at 0.05 eV incidence translational energy.[22] With the newly won knowledge of the lessons learned from this work, we have repeated IESH modeling under the conditions of Ref. 22, but with multi-bounce collisions removed as we have done in this paper. This reveals a substantially reduced vibrational inelasticity, degrading the apparent good agreement with experiment. While NO on Au(111) remains one of the best understood examples of electronically nonadiabatic energy transfer and while IESH still represents the gold standard for electronically nonadiabatic dynamical treatment, it appears that input data to IESH (namely, the adiabatic potential energy surface and the electronically nonadiabatic couplings, both of which are derived from DFT) are not yet of sufficient accuracy to yield good agreement with experiment. Future developments, for example, using embedded correlated wave function methods,[46] may provide the most productive path forward.

ACKNOWLEDGMENTS

We thank Dr. Neil Shenvi and Professor John Tully for many fruitful discussions during the preparation of this manuscript. A.M.W. and D.J.A. acknowledge support from the Alexander von Humboldt foundation.

APPENDIX A: CLASSICAL VIBRATIONAL ENERGY DISTRIBUTIONS

Classical (non-quantized) vibrational energy distributions for an incidence energy $E_i = 0.4$ eV, as directly obtained from the simulations, are presented in Figure 9. We compare the results of (1) IESH simulations, (2) IESH simulations after selection of single-bounce trajectories, (3) IESH simulations after selection of multi-bounce trajectories, and (4) an adiabatic model in the upper figure. Similarly, the lower figure shows the results of EF simulations, EF simulations after selection of single-bounce trajectories, and EF simulations after selection of multi-bounce trajectories. As expected, the adia-

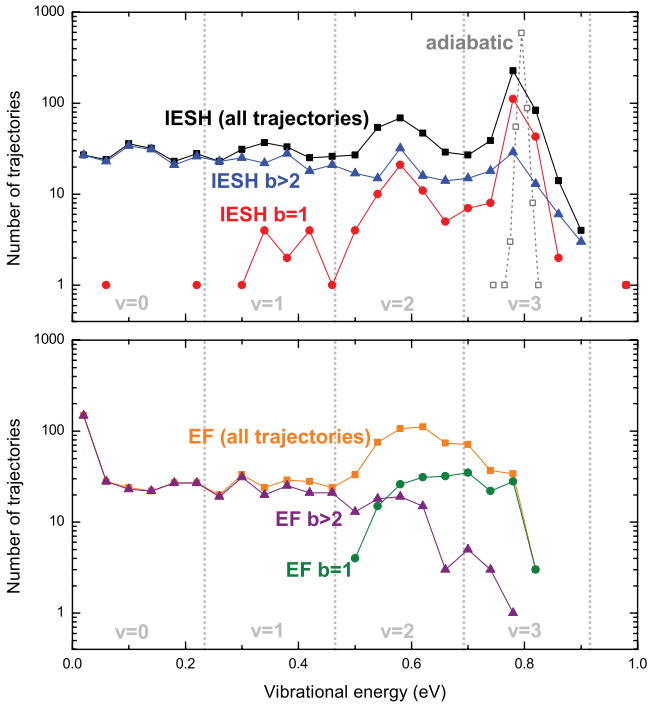

FIG. 9. The top figure shows classical vibrational energy distributions for IESH (black squares), IESH after selection of single-bounce trajectories ($b = 1$, red circles), IESH after selection of multi-bounce trajectories ($b > 2$, blue triangles), and for an adiabatic simulation (gray open squares). The bottom figure shows similar distributions for EF simulations (all trajectories: orange squares; $b = 1$: green circles; $b > 2$: purple triangles). The bins for quantized vibrational states $v = 0,\ 1,\ 2,\ 3$ are indicated by the vertical dotted lines. The initial vibrational energy was set to $E_{\mathrm{vib}}{}^{0} = 0.80$ eV, corresponding to $v = 3$. The incidence translational energy is $E_i = 0.4$ eV. For both IESH and EF simulations, a number of 1000 trajectories were simulated. We find that vibrational relaxation is insignificant for the adiabatic simulation, whereas both IESH and EF predict substantial relaxation. Selecting only single-bounce or only multi-bounce trajectories has a drastic influence on the resulting vibrational energy distributions. For EF, the selection of single-bounce trajectories completely suppresses the relaxation into $v = 1$ and $v = 0$.

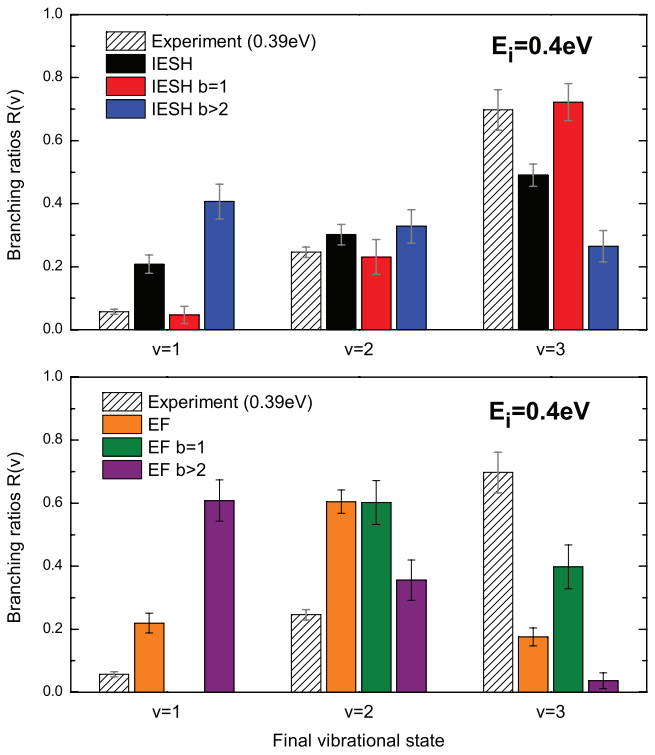

FIG. 10. Branching ratios for vibrational states $v = 1,\ 2,\ 3$ in histogram form. We compare experimental data (hatched bars) to IESH simulations (top) with all trajectories (black), after selection of single-bounce trajectories ($b = 1$, red) and after selection of multi-bounce trajectories ($b > 2$, blue), and similarly to EF simulations (bottom; all trajectories: orange; $b = 1$: green; $b > 2$: purple). The incidence translational energy is $E_i = 0.39$ eV for the experimental data and $E_i = 0.4$ eV for the simulations. For both IESH and EF, the selection of single-bounce trajectories leads to reduced relaxation, whereas the selection of multi-bounce trajectories leads to enhanced relaxation. Only the IESH simulation with a restriction to single-bounce trajectories is in good agreement with the experimental data; however, the agreement is not quantitative for all incidence energies.

batic simulation does not predict significant redistribution of vibrational energy. It will thus be no longer considered.

In contrast to the adiabatic picture, the IESH simulation predicts strong relaxation of vibrational energy even to values near $\hbar\omega_e/2 = 0.12$ eV, corresponding to the zero-point energy of the quantized NO vibration. Selecting the subset of single-bounce trajectories and applying the same analysis, we find considerably weaker relaxation of vibrational energy, in particular at vibrational energies corresponding to the $v = 0$ and $v = 1$ states. Significant relaxation to vibrational energies corresponding to $v = 2$ is however still observed. From this analysis, it is evident that the strongest vibrational relaxation is exclusively due to multi-bounce trajectories. Removing them from the analysis changes the resulting vibrational energy distribution quite drastically.

The EF calculations predict even stronger vibrational relaxation than IESH, particular relaxation by one vibrational quantum, i.e., into $v = 2$. In addition, there is considerably more relaxation to vibrational energies near zero. The selection of single-bounce trajectories completely suppresses relaxation into $v = 1$ and $v = 0$. The corresponding quantized vibrational state distributions were calculated using the box binning procedure, as explained in Sec. II. The resulting branching ratios for the $v = 1,\ 2,\ 3$ channels are shown in histogram form in Figure 10, along with experimental data for $E_i = 0.39$ eV. We again find that the selection of multi-bounce trajectories leads to enhanced relaxation, whereas the selection of single-bounce trajectories leads to reduced relaxation. Only the IESH simulation with selection of single-bounce trajectories agrees with experiment. For the single-bounce EF simulation, the $v = 3$ survival probability is only ≈40%, which clearly disagrees with the experimental data.

APPENDIX B: DETAILED ANALYSIS OF z_{min} AND θ_{min} DISTRIBUTIONS

The z_{min} and θ_{min} distributions (histograms) for several incidence energies are shown in Figure 11. We find that for incidence energies below ≈0.4 eV, the z_{min} distribution develops an extra peak at very small values, $z_{\mathrm{min}} \leq 1.2$ Å. The inset diagram (for $E_i = 0.3$ eV) shows that this extra peak is exclusively caused by multi-bounce trajectories. For θ_{min}, we find qualitatively similar but less pronounced behavior. The fraction of molecules with $\theta_{\mathrm{min}} > 160°$ (near N-down orientation) clearly increases as the incidence energy is decreased,

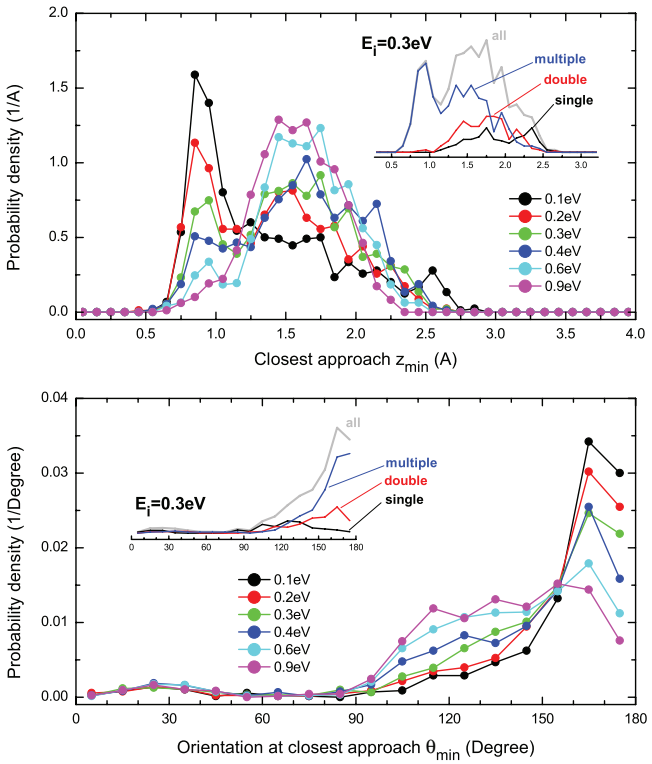

FIG. 11. Distributions for z_{min} (top) and θ_{min} (bottom) at various incidence energies. Top: In addition to a broad feature at 1.2 Å $< z_{min} <$ 2.5 Å, the distributions develop an extra peak, at small values $z_{min} <$ 1.2Å, at smaller incidence energies. The inset diagram presents the distribution for $E_i = 0.3$ eV along with the distributions for single, double, and multiple bounce collisions, clearly showing that the extra peak is exclusively due to multi-bounce collisions. Bottom: The corresponding analysis for θ_{min} shows that for low incidence energies, the distributions shift toward 180° (N-down) orientation, but no clear separation is observed as for the z_{min} distributions. The inset diagram shows that for multi-bounce trajectories, the distributions are narrower and shifted toward 180° as compared to those for single and double-bounce collisions.

and again the inset diagram shows that those orientations are mostly caused by multi-bounce trajectories.

[1]M. Born and R. Oppenheimer, "Zur Quantentheorie der Molekeln," Ann. Phys. **389**, 457–484 (1927), published in English online in 2006.
[2]A. M. Wodtke, J. C. Tully, and D. J. Auerbach, Int. Rev. Phys. Chem. **23**, 513–539 (2004).
[3]C. Bartels, R. Cooper, D. J. Auerbach, and A. M. Wodtke, Chem. Sci. **2**, 1647–1655 (2011).
[4]I. Rahinov, R. Cooper, D. Matsiev, C. Bartels, D. J. Auerbach, and A. M. Wodtke, Phys. Chem. Chem. Phys. **13**, 12680–12692 (2011).
[5]M. Morin, N. J. Levinos, and A. L. Harris, J. Chem. Phys. **96**, 3950–3956 (1992).
[6]J. D. Beckerle, M. P. Casassa, R. R. Cavanagh, E. J. Heilweil, and J. C. Stephenson, Phys. Rev. Lett. **64**, 2090–2093 (1990).
[7]M. Bonn, C. Hess, S. Funk, J. H. Miners, B. N. J. Persson, M. Wolf, and G. Ertl, Phys. Rev. Lett. **84**, 4653–4656 (2000).
[8]H. C. Chang and G. E. Ewing, Phys. Rev. Lett. **65**, 2125–2128 (1990).
[9]B. N. J. Persson and M. Persson, Solid State Commun. **36**, 175–179 (1980).
[10]J. C. Tully, M. Gomez, and M. Head-Gordon, J. Vac. Sci. Tech. A **11**, 1914–1920 (1993).
[11]C. T. Rettner, F. Fabre, J. Kimman, and D. J. Auerbach, Phys. Rev. Lett. **55**, 1904–1907 (1985).
[12]E. K. Watts, J. L. W. Siders, and G. O. Sitz, Surf. Sci. **374**, 191–196 (1997).
[13]Q. Ran, D. Matsiev, D. J. Auerbach, and A. M. Wodtke, Phys. Rev. Lett. **98**, 237601 (2007).
[14]T. Schäfer, N. Bartels, K. Golibrzuch, C. Bartels, H. Köckert, D. J. Auerbach, T. N. Kitsopoulos, and A. M. Wodtke, Phys. Chem. Chem. Phys. **15**, 1863–1867 (2013).
[15]D. M. Newns, Surf. Sci. **171**, 600–614 (1986).
[16]Y. H. Huang, C. T. Rettner, D. J. Auerbach, and A. M. Wodtke, Science **290**, 111–114 (2000).
[17]S. Li and H. Guo, J. Phys. Chem. **117**, 4499 (2002).
[18]S. Monturet and P. Saalfrank, Phys. Rev. B **82**, 075404 (2010).
[19]J. C. Tully, J. Chem. Phys. **93**, 1061–1071 (1990).
[20]S. Roy, N. A. Shenvi, and J. C. Tully, J. Chem. Phys. **130**, 174716 (2009).
[21]N. Shenvi, S. Roy, and J. C. Tully, J. Chem. Phys. **130**, 174107 (2009).
[22]N. Shenvi, S. Roy, and J. C. Tully, Science **326**, 829–832 (2009).
[23]R. Cooper, Z. Li, K. Golibrzuch, C. Bartels, I. Rahinov, D. J. Auerbach, and A. M. Wodtke, J. Chem. Phys. **137**, 064705 (2012).
[24]R. Cooper, I. Rahinov, Z. S. Li, D. Matsiev, D. J. Auerbach, and A. M. Wodtke, Chem. Sci. **1**, 55–61 (2010).
[25]K. Golibrzuch, A. Kandratsenka, I. Rahinov, R. Cooper, D. J. Auerbach, A. M. Wodtke, and C. Bartels, J. Phys. Chem. A **117**, 7091–7101 (2013).
[26]R. Cooper, C. Bartels, A. Kandratsenka, I. Rahinov, N. Shenvi, K. Golibrzuch, Z. S. Li, D. J. Auerbach, J. C. Tully, and A. M. Wodtke, Angew. Chem. Int. Ed. **51**, 4954–4958 (2012).
[27]Y. Huang, A. M. Wodtke, H. Hou, C. T. Rettner, and D. J. Auerbach, Phys. Rev. Lett. **84**, 2985–2988 (2000).
[28]H. Falsig, J. Shen, T. S. Khan, W. Guo, G. Jones, S. Dahl, and T. Bligaard, "On the structure sensitivity of direct NO decomposition over low-index transition metal facets," Top. Catal. (published online).
[29]Q. Ran, D. Matsiev, A. M. Wodtke, and D. J. Auerbach, Rev. Sci. Instrum. **78**, 104104 (2007).
[30]K. Golibrzuch, P. R. Shirhatti, J. Altschaffel, I. Rahinov, D. J. Auerbach, A. M. Wodtke, and C. Bartels, J. Phys. Chem. A **117**, 8750–8760 (2013).
[31]P. W. Anderson, Phys. Rev. **124**, 41 (1961).
[32]D. M. Newns, Phys. Rev. **178**, 1123 (1969).
[33]M. Head-Gordon and J. C. Tully, J. Chem. Phys. **103**, 10137–10145 (1995).
[34]G. D. Billing, *Dynamics of Molecule Surface Interactions* (Wiley, New York, 2000).
[35]R. Spindler, L. Isaacson, and T. Wentink, J. Quant. Spectrosc. Radiat. Transf. **10**, 621–628 (1970).
[36]J. Hurst, L. Wharton, K. Janda, and D. Auerbach, J. Phys. Chem. **78**, 1559 (1983).
[37]C. Rettner, J. Kimman, and D. Auerbach, J. Phys. Chem. **94**, 734 (1991).
[38]A. M. Wodtke, H. Yuhui, and D. J. Auerbach, Chem. Phys. Lett. **413**, 326–330 (2005).
[39]J. C. Tully and R. K. Preston, J. Phys. Chem. **55**, 562 (1971).
[40]G. Begbie and M. Born, Proc. R. Soc. London, Ser. A **188**, 179–188 (1947).
[41]G. Begbie, Proc. R. Soc. London, Ser. A **188**, 189–208 (1947).
[42]G. Gilat and R. Nicklow, Phys. Rev. **143**, 487 (1966).
[43]J. Lynn, H. Smith, and R. Nicklow, Phys. Rev. B **8**, 3493 (1973).
[44]N. Bartels, K. Golibrzuch, C. Bartels, L. Chen, D. J. Auerbach, A. M. Wodtke, and T. Schäfer, Proc. Natl. Acad. Sci. U.S.A. **110**, 17738–17743 (2013).
[45]F. Libisch, C. Huang, P. Liao, M. Pavone, and E. A. Carter, Phys. Rev. Lett. **109**, 198303 (2012).
[46]C. Huang, M. Pavone, and E. A. Carter, J. Chem. Phys. **134**, 154110 (2011).